Biomass and Bioenergy 192 (2025) 107496

Contents lists available at ScienceDirect

Biomass and Bioenergy

journal homepage: www.elsevier.com/locate/biombioe

Preparation and electrochemical properties of modified biochar

Yang Sun [a], Qianqian Yu [a], Tianhua Yang [b,*], Rundong Li [a], Shiyu Zhao [a]

[a] School of Energy and Environment, Liaoning Province Key Laboratory of Clean Energy, Shenyang Aerospace University, Shenyang, 110036, China
[b] School of Energy and Environment, Liaoning Province Key Laboratory of Clean Energy, Shenyang Aerospace University, China

ARTICLE INFO

Keywords:
Biochar
Modification
Specific surface area
Electrochemical properties

ABSTRACT

High-performance biochar-based supercapacitors extremely depend on the reasonable microstructure of electrode materials, so optimizing pore structure and surface properties is an important research topic. In this paper, HNO_3 and H_2O_2 were used to modify wood chip biochar, which enhanced the oxygen-containing functional groups of biochar and optimized the pore size distribution. NPCBC-45 and HPCBC-20 micropore sizes were concentrated at 0.92 nm and 0.90 nm, respectively, and the mesoporosity was 33 % and 65 %, respectively. The supercapacitors using NPCBC-45 and HPCBC-20 as electrodes exhibited excellent specific capacitance, reaching 338.88 $F•g^{-1}$ and 165 $F•g^{-1}$, respectively, which were increased by 137.39 % and 15.59 %, respectively. The prepared double-layer capacitor showed good cycle stability, and the cycle efficiency was 94 % after 2000 cycles. Therefore, the results of this study show that HNO_3 and H_2O_2 have application value in optimizing the microstructure of carbon material electrodes.

1. Introduction

With the rapid development of the world economy and increasing demand for energy, the rapid depletion of fossil energy and a series of environmental pollution problems have become important challenges facing the world today. To tackle this problem, countries around the world have begun to develop clean renewable energy sources such as solar or wind energy [1]. However, the energy obtained from renewable energy sources such as wind, hydro and solar energy has problems such as intermittency and uncertainty, making it challenging to grid-connected power generation [2]. So it is necessary to find out efficient energy storage and conversion systems. As one of the positive efficient energy storage devices, supercapacitors have recently attracted great interest from researchers around the world [3–5].

Electrode materials are one of the key factors determining the performance of supercapacitors [6–8]. Porous carbon-based materials are ideal electrode materials of supercapacitor with excellent performance due to their high specific surface area, developed pore structure, high carbon content, excellent conductivity and high chemical stability. Biochar is prepared from a variety of agricultural and forestry residues, and its preparation can transform waste into resources and reduce the amount of solid waste [9–11].

According to the different energy storage mechanism, supercapacitors can be divided into electric double-layer capacitors (EDLCs) and pseudocapacitance [12,13]. The cycle life of pseudocapacitors is low due to the electrochemical reaction within the entire electrode [14,15]. EDLCs is physical batteries that storage and release energy based on the electric double-layer effect, and have ultra-high cycle life and high power density due to its physical structure [16]. However, because the electric double-layer behavior is only generated on the surface of the carbon material electrode, the energy density of EDLCs is much lower than that of the pseudocapacitance [17]. In order to overcome these problems, the energy density of biochar supercapacitors can be enhanced by modifying methods [18–20]. Wei et al. used ammonium chloride modified corncob to prepare biochar, specific surface area was increased up to 1440.3 $m^2 g^{-1}$. The specific capacity of modified biochar is up to 175 $F•g^{-1}$ at 0.5 $A•g^{-1}$ [21]. Modification is one of the effective means to change the surface chemical properties of biochar. The number and diversity of surface functional groups of biochar are enhanced by modification, which significantly improves the electrochemical performance of biochar [22,23]. Generally, the content of N and O groups of biochar prepared is not high, and these groups directly affect the surface chemical properties of carbon materials. The modification process can doping a variety of functional groups onto the surface of biochar [24–26], and these groups will undergo reversible oxidation-reduction reaction (REDOX) with electrolyte ions in the electrolyte to increase the electric capacity. Rawat et al. used CO_2 as activator, the oxygen-containing groups of litchi seed biochar were increased, and the

* Corresponding author. No.37 Daoyi south street, Daoyi Economic Development district, Shenyang Liaoning province, 110136, China.
E-mail address: sunyang@sau.edu.cn (T. Yang).

https://doi.org/10.1016/j.biombioe.2024.107496
Received 14 October 2024; Received in revised form 17 November 2024; Accepted 18 November 2024
Available online 26 November 2024

specific capacitance of carbon material was increased [27]. Sylla et al. used melamine as nitrogen source to prepare non-in-situ nitrogen-doped peanut shell porous carbon, which improved the capacitive performance and capacitor stability [28].

The process of doping oxygen-containing functional groups on the surface of materials is called oxidation [29], and the contents of carbonyl, carboxyl, phenolic and lactone groups on the surface of biochar can be improved by the modification of oxidants. The oxygen-containing functional groups increase the electronegativity of biochar and increase the electrolyte ions to undergo highly reversible REDOX reactions. Nitric acid and hydrogen peroxide are often used as oxidizing agents. In this paper, the oxidizing agents above modified biochar surface, and their effects on the apparent morphology, pore size structure and electrochemical properties of biochar were investigated. This study explored an effective method to prepare high-performance biochar, and provided a new strategy for the resource utilization of pine sawdust waste.

2. Experiments and materials

2.1. Materials

Pine chips from a wood yard near Shenbei New District, Shenyang City, Liaoning Province were selected. The pine chips were repeatedly cleaned with water, and then the clean pine chips were put into a dryer to dry, and the powder was screened by a 100-mesh screen after pulverized. The proximate and ultimate analysis of biomass were tested, with specific data shown in Table 1.

2.2. Preparation and modification of the biochar

Carbon material electrodes are prepared by using the biochar obtained above, and the specific test scheme is as follows:

A certain amount of anhydrous ethanol was dropped into a certain amount of 60 % PTFE emulsion (Japan Daijin), and the PTFE emulsion was broken and diluted by ultrasound for 120 min. Biochar, binder and conductive agent (purity ≥99.9 %, Guangdong Candle New Energy Technology Co., LTD.) were mixed at the ratio of 8:1:1 and treated with ultrasonic wave for 150min to further disperse evenly. The nickel foam (purity ≥99.9 %, Kunshan New Material Co., LTD.) was ultrasonic cleaned with propyl alcohol and anhydrous ethanol for 5 min to remove the surface oil, and then ultrasonic cleaned with 2 M HCl for 5 min to remove the surface oxidation layer, and the residual hydrochloric acid was cleaned with deionized water. After drying, the nickel foam was cut into 1 cm × 2 cm strips, weighed and recorded as m_1 for use. The biochar mixture above was evenly dropped on nickel foam with a pipette gun. After drying, the biochar mixture was pressed on a tablet press at 10 MPa pressure for 1 min and weighed as m_2 for use. The mass of biochar was calculated using formula 1.

$$\text{Mass of biochar} = (m_1\text{-}m_2) \times 0.8 \quad (1)$$

Electrochemical tests were conducted on electrochemical workstation (CHI760E, Shanghai Chenhua) and battery tester (CT-4008t Shenzhen Xinwei Electronics). The experiments were carried out with three-electrodes and symmetrical double electrode system with 3M KOH electrolyte solution. Cyclic voltammogram (CV) and galvanostatic charge-discharge (GCD) were obtained using 3M KOH as an electrolyte solution in a potential window range of – 0.1 to 0.9 V vs Pt/HgO with different scan rates (10 mV s^{-1}, 25 mV s^{-1}, 50 mV s^{-1} and 100 mV s^{-1} respectively) and current density (1 A g^{-1}, 5 A g^{-1} and 10 A g^{-1} respectively). Electrochemical impedance spectroscopy (EIS) was carried out in the frequency range 0.01 Hz–10 kHz. The specific capacitance (C_m, F·g^{-1}) was calculated by the following formula [27].

$$C_m = \frac{I}{m \times v} \quad (2)$$

Where, v and m were the scan rate (V·s^{-1}) and mass of the active material in the electrodes (g), respectively.

3. Results and discussion

3.1. Structural characterization of modified biochar

3.1.1. Specific surface area and pore size distribution

N_2 adsorption and desorption isothermal of modified biochar were tested, as shown in Fig. 1. The results shows that the modified biochar conforms to the type I isotherm defined by International Union of Pure and Applied Chemistry (IUPAC), which reflects the micropore filling phenomenon on the micropore adsorbent, indicating that the biochar has a rich micropore structure [30]. HPCBC-20 has obvious hysteresis, which indicates that HPCBC-20 has abundant mesoporous structure [31]. The nitrogen adsorption capacity of all samples decreased, indicating that the nitrogen adsorption capacity of biochar decreased to different degrees after modification. Fig. 1(a) after HNO_3 modification, the nitrogen adsorption capacity of biochar decreased significantly. With the variation of HNO_3 concentration, the change in the adsorption amount of biochar was not obvious, suggesting that the concentration of HNO_3 has a relatively small influence on the nitrogen adsorption capacity of biochar. Fig. 1(b) after H_2O_2 modification, the nitrogen adsorption capacity of biochar decreased significantly. With the increase of H_2O_2 concentration, the nitrogen adsorption capacity of biochar began to increase, indicating that H_2O_2 concentration can affect the nitrogen adsorption capacity of materials.

From Fig. 2(a) and (b), it can be found that the specific surface area (SSA) and pore volume of biochar decreased after HNO_3 modification. The average pore size and mesoporous pore capacity of the sample NPCBC-60 were increased, which was due to the high concentration of HNO_3, and the micropores of biochar were further transformed into mesoporous pores by etching and re expanding. The micropore volume of samples NPCBC-30 and NPCBC-45 increased, while the micropore volume of sample NPCBC-60 decreased slightly, indicating that HNO_3 can etch biochar to generate new micropores. After modification of H_2O_2 as shown in Fig. 2(a) and (b), the specific surface area of biochar decreased and the micropore volume increased. The total pore volume and mesoporous pore volume of samples HPCBC-10 and HPCBC-20 increased, and the decomposition rate of H_2O_2 at low concentration was slow under the condition of shock. H_2O_2 molecules could be immersed into the pore structure of biochar to separate into oxygen, further broadening the mesoporous structure of biochar. With the increase of H_2O_2 concentration, the decomposition rate of H_2O_2 is intensified, and it cannot penetrate into the interior of biochar, but can only decompose on the surface of biochar. Therefore, the pore structure of sample HPCBC-30 does not change significantly.

It can be found from Fig. 3(a) aperture distribution that after surface modification of HNO_3, the micropore distribution of samples NPCBC-30, NPCBC-45 and NPCBC-60 is 0.9–0.94 nm, 0.91–0.92 nm and 0.91–0.93

Table 1
Proximate and ultimate analysis of pine chips.

Sample	Proximate analysis *ad w* %				Ultimate analysis *ad w* %				
	M	A	V	FC	C	H	O	N	S
pine chips	5.60	0.79	83.93	9.68	51.03	6.44	41.08	0.55	0.11

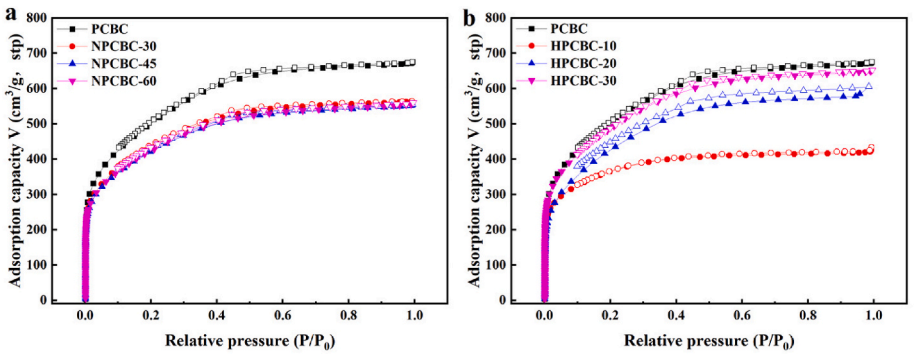

Fig. 1. N_2 adsorption and desorption isothermal (a) NPCBC, (b) HPCBC.

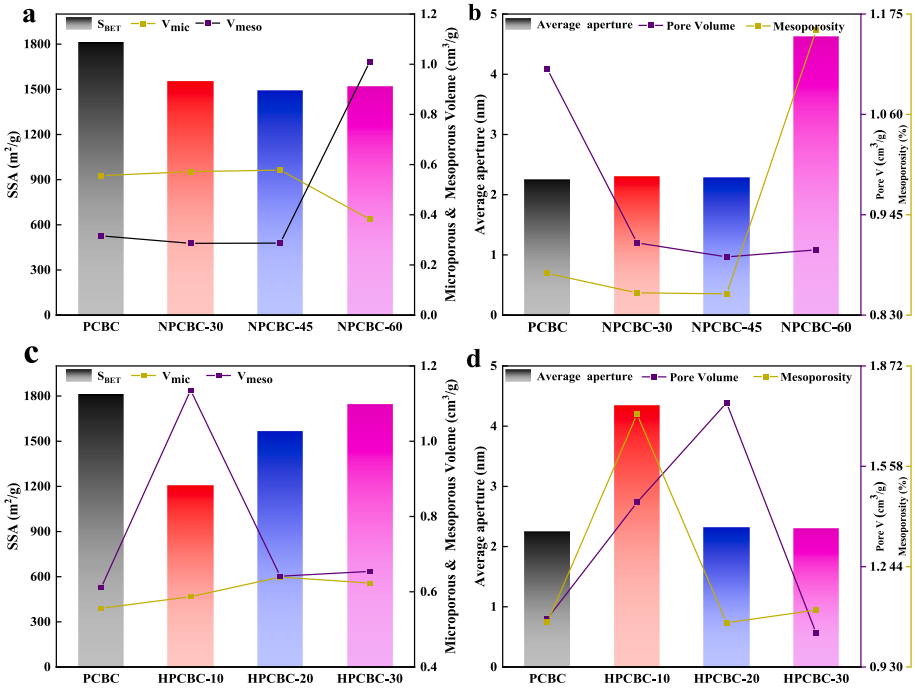

Fig. 2. (a, b) SSA, pore volume and average aperture size of NPCBC, (c, d) SSA, pore volume and average aperture size of HPCBC.

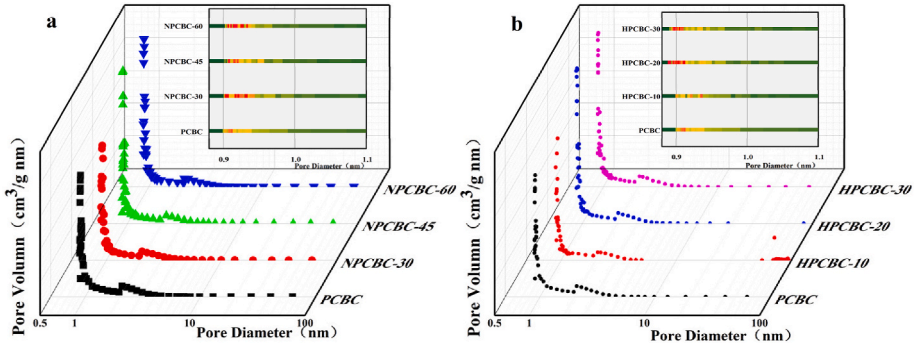

Fig. 3. Pore size distribution of modified biochar (a) NPCBC, (b) HPCBC.

nm, respectively, and the mesoporous distribution of the three samples is similar to that of PCBC. HNO_3 can penetrate into the interior of biochar, react with amorphous carbon, generate new defect sites, and further modify existing micropores, thus affecting the micropore distribution of biochar. Fig. 3(b) after surface modification of H_2O_2, the micropores of HPCBC-10, HPCBC-20 and HPCBC-30 are distributed in 0.93–0.94 nm, 0.99–0.91 nm and 0.90–0.91 nm, respectively. The mesoporous distribution between 5 and 40 nm in sample HPCBC-10 was destroyed. This is due to the low concentration of H_2O_2, which can be immersed into the mesoporous 5–40 nm inside biochar, and violent oxidative decomposition reaction occurs under the reduction of elemental carbon, resulting in the diffusion of oxygen, resulting in

mesoporous collapse. The mesoporous distribution of 20–80 nm in sample HPCBC-20 was destroyed. With the increase of H_2O_2 concentration, the reaction between H_2O_2 and carbon is advanced, the reaction degree is intensified, and a large amount of oxygen is produced in a short time. When a large amount of oxygen escapes in a short time, it destroys the mesoporous structure of biochar and generates new defect sites to form fine microporous structures. With the further increase of H_2O_2 concentration, H_2O_2 oxidized and decomposed on the surface of sample HPCBC-30 or in the macropore channel, and could not be further immersed in the mesoporous structure of biochar. Therefore, high concentration of H_2O_2 has the least effect on the pore size distribution of biochar.

In summary, the specific surface area of the modified biochar decreased, and the mesoporous ratios of samples NPCBC-45, HPCBC-20 were close to 30 %. The pore structure was improved and the distribution of micropores became more uniform. Therefore, the pore structure of biochar can be further regulated by changing the concentration of chemical reagents.

3.1.2. Graphitization degree analysis

XRD patterns and Raman spectroscopy of the modified biochar are shown in Fig. 4. As can be seen from Fig. 4(a), the biochar structure could be reflected by the obvious diffraction peaks of (002) crystal face and dwarf peaks of (100) crystal face, which were around at $2\theta = 25^{\circ}$ and $2\theta = 44^{\circ}$, respectively [32], indicating that the biochar presents different degrees of graphitization. After modification, the diffraction peak of biochar did not change significantly, indicating that the modification had little effect on the graphitization degree of biochar. For Raman spectra, the G and D band were reflected by two peaks around at 1590 $cm^{-1}$and 1350 cm^{-1}, respectively, and the graphitization degree of biochar can be represented by the intensity ratio between G and D band (I_G/I_D) [29]. It can be seen from Fig. 4(c) and (d) and Table 2 that the degree of graphitization after modification of biochar does not change significantly compared with that before modification, and the degree of crystallinity decreases. Modification methods of HNO_3 and H_2O_2 can etch the carbon skeleton of biochar and reduce the crystallinity of biochar (see Table 3).

Table 2
Sub-peak fitting of D-peak and G-peak Raman spectra.

	D-peak		G-peak		ID/IG
	Area	High	Area	High	
PCBC	0.158	0.292	0.348	0.345	0.87
NPCBC	0.565	0.390	0.261	0.435	0.89
HPCBC	0.489	0.355	0.224	0.376	0.94

Table 3
Sub-peak fitting of 1180 and 1510 Raman spectra.

	1180		1510		sp^3carbon A^3_{sp}/A^2_{sp}
	Area	High	Area	High	
PCBC	0.325	0.120	0.169	0.244	1.07
NPCBC	0.115	0.064	0.058	0.112	0.47
HPCBC	0.180	0.121	0.107	0.149	0.50

3.1.3. Elemental analysis and oxygen-containing functional groups

As can be seen from Fig. 5, after HNO_3 modification, the content of oxygen element in biochar increased, and the content of oxygen element increased with the increase of HNO_3 concentration. HNO_3 is a strong oxidizing agent and is corrosive at the same time. It strongly corrodes the internal pores of biochar, changes its pore size structure, and forms a large number of oxygen-containing functional groups in the internal pores of biochar. After H_2O_2 modification, the oxygen content of biochar increased, and the oxygen content decreased with the increase of H_2O_2 concentration.H_2O_2 is a strong oxidizing agent that is easily decomposed, and the higher the concentration, the easier it is to decompose. H_2O_2 cannot penetrate deep into the pore structure of biochar, and is oxidized and decomposed on the outer surface of biochar. The higher the concentration of H_2O_2, the more outward the decomposition position becomes, which cannot effectively corrode the micropore structure of biochar, and the ability of incorporating oxygen-containing functional groups on the surface of biochar is weak.

As shown in the Fig. 6, the infrared spectrum of biochar indicates oxygen-containing functional groups in the range of 900–1400 cm^{-1},

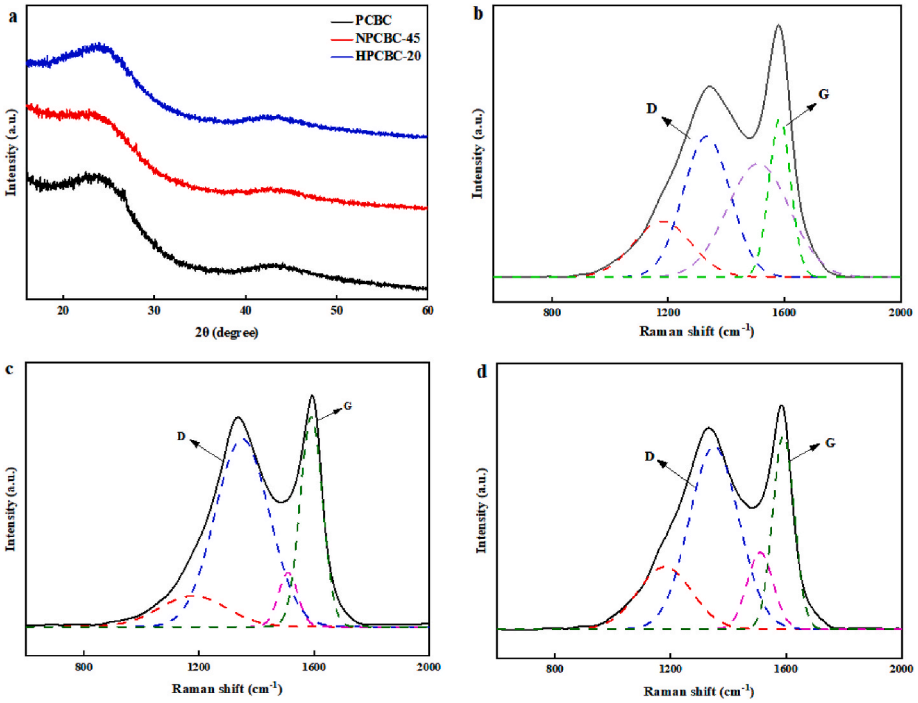

Fig. 4. XRD pattern (a) and Raman spectra of PCBC (b), NPCBC (c), HPCBC (d).

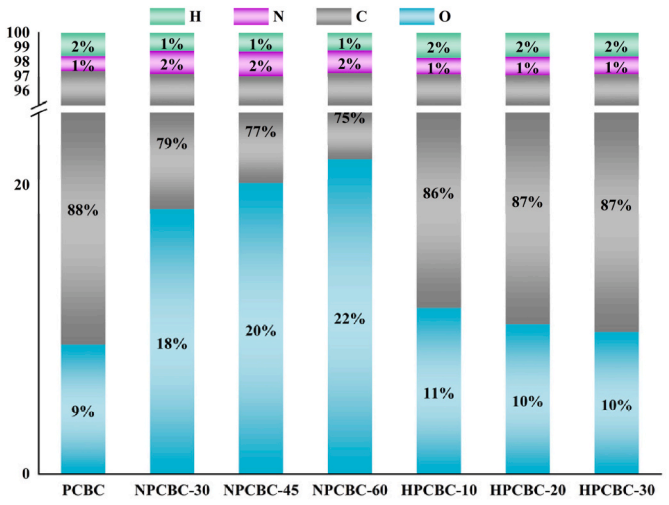

Fig. 5. Elements analysis of modified biochar.

aromatic ring skeleton in the range of 1450–1650 cm^{-1}, carbonyl group in the range of 1650–1900 cm^{-1}, and alcohol hydroxyl group in the range of 3300–3600 cm^{-1} [33]. Due to the complex types of oxygen-containing functional groups of activated carbon, the phenomenon of peak superposition appears on the atlas. To analyze the oxygen-containing functional groups of activated carbon, the distribution of each oxygen-containing functional group can be obtained by peak splitting and Gaussian fitting for 900-1400 cm^{-1} of the spectrum.

Fig. 7(b)–(d) after HNO_3 modification, the types and contents of oxygen-containing functional groups of biochar increased, and with the increase of HNO_3 concentration, the types of oxygen-containing functional groups decreased. A large number of aromatic oxygen-containing functional groups appeared in sample NPCBC-10, such as hydroxyl, ether, aromatic ether, aldehydes, ester groups, lactone groups, etc. With the increase of HNO_3 concentration, the types of oxygen-containing functional groups of biochar decreased and the content increased, and there were phenols, ketone and ester groups. Fig. 7(e) - (f) after H_2O_2 modification, biochar appeared phenols, ester groups and hydroxyl groups.

In order to reveal the change mechanism of the existence form of oxygen element, XPS test was carried out on the modified biochar, and the content of oxygen-containing functional groups in each sample was shown in Fig. 7(h). It can be found that after the modification of biochar, the oxygen element exists in the form of C=O, C-O and C-O-C [34]. After HNO_3 modification, the C=O content in biochar increases, which can provide more pseudo capacitance for biochar and increase the specific capacitance of biochar. After H_2O_2 modification, C-O-C in biochar is oxidized to C=O, resulting in a decrease in the infiltration of biochar.

3.2. Electrochemical analysis of modified biochar

3.2.1. CV curve analysis

With 3 M KOH as electrolyte, the electrochemical performance of modified biochar was evaluated by using a three-electrode system, which was shown in Fig. 8. All the CV curve shape of modified biochar did not change significantly at scanning rates of 10 mV s^{-1}, 25 mV s^{-1}, 50 mV s^{-1} and 100 mV s^{-1}. The results suggested that the modified biochar had better rate performance. The ideal double-layer capacitor CV curve is quasi-rectangular shape. However, in this experiment, the CV curves of the modified biochar electrode was slightly deformed. The reason was that the charge distribution inside the biochar electrode was dispersed, and there was a difference in the resistance of the electrolyte at the top and bottom of the biochar micropores, which causes the electrolyte ions to move faster at the top of the micropores than at the bottom. On the other hand, there was an ohmic voltage drop in the biochar electrode. The above two aspects worked together to cause the biochar electrode to have a dispersed capacitance effect, causing the CV curve to be deformed. The CV curves of the modified biochars show a convex scanning response current platform at a high scan rate, and a wide peak representing pseudo capacitance appears, indicating that REDOX reactions occur during the charge and discharge process, and providing Faraday pseudo capacitance. This indicated that oxygen-containing functional groups on the surface of biochar participate in the electrochemical reaction and provide additional capacitance.

3.2.2. GCD curve and cycle efficiency stability analysis

It can be seen from Fig. 9(a) that the constant current charge-discharge curves of modified biochar maintain an approximate "isosceles triangle" shape, indicating that modified biochar has good charge-discharge reversibility and electrochemical performance [35]. The sample NPCBC-45 shown in Fig. 9(b) has a low "voltage drop", indicating that the series resistance of the sample is small, and Fig. 9(c) the "voltage drop" of sample HPCBC-20 is more obvious, indicating that the series resistance of the sample is increased. After the modification of HNO_3 and H_2O_2, the cyclic charge-discharge curve of biochar did not change significantly under the condition of high current density, indicating that the modified biochar had good magnification performance.

NPCBC-45 is selected as the electrode material to install the battery buckle, and the installed battery buckle is tested for cyclic charge and discharge, as shown in Fig. 9(d). In the process of 2000 cycles, the cycle efficiency increases gradually from 1 to 60 times, reaching 106 %. With the gradual increase in the number of cycles, the cycle stability gradually decreases. At 2000 cycles, its cycle efficiency is about 94 %, and the corresponding power density is 33.4 W/kg.

Based on the constant current charge-discharge curve, the specific capacitance and energy density equivalent series internal resistance of biochar were calculated respectively. As shown in Table 4, the specific capacitance of modified biochar was significantly improved compared with that before modification, and the specific capacitance of sample

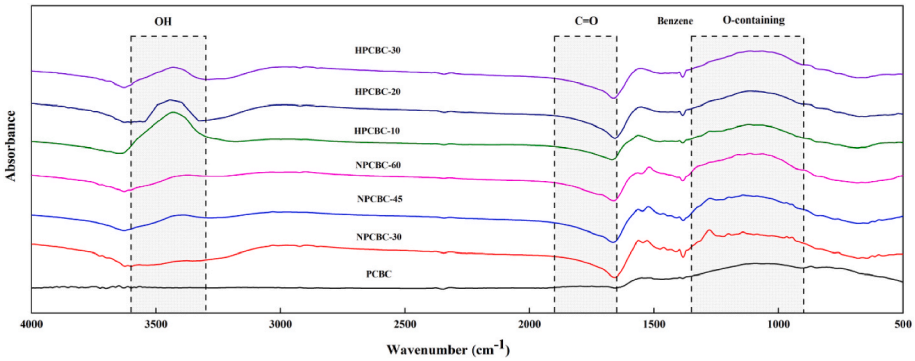

Fig. 6. FTIR analysis of modified biochar.

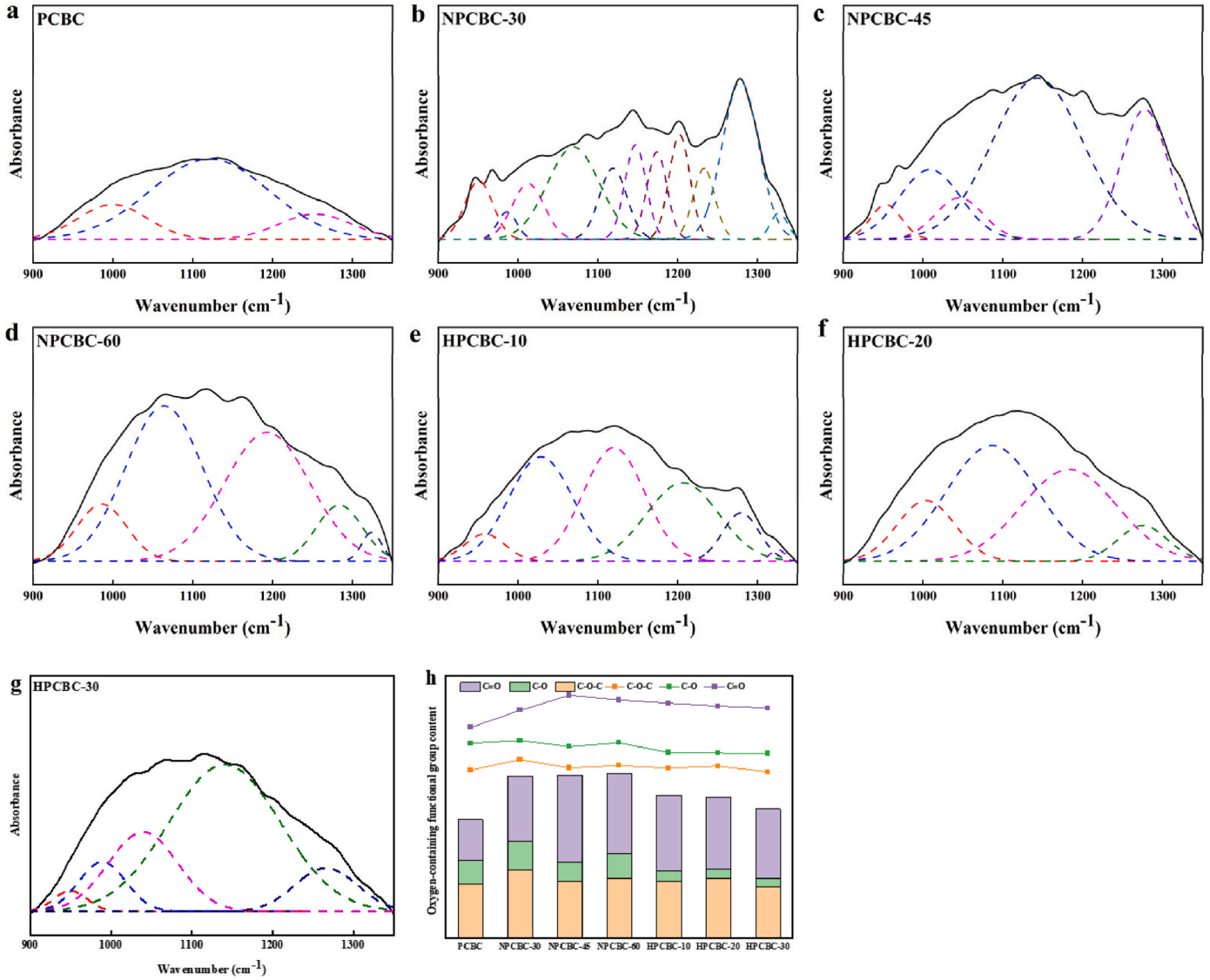

Fig. 7. Infrared Gaussian fitting (a) PCBC, (b)(c)(d) NPCBC, (e)(f)(g) HPCBC, (h) Content of oxygen-containing functional groups after XPS fitting of modified biochar.

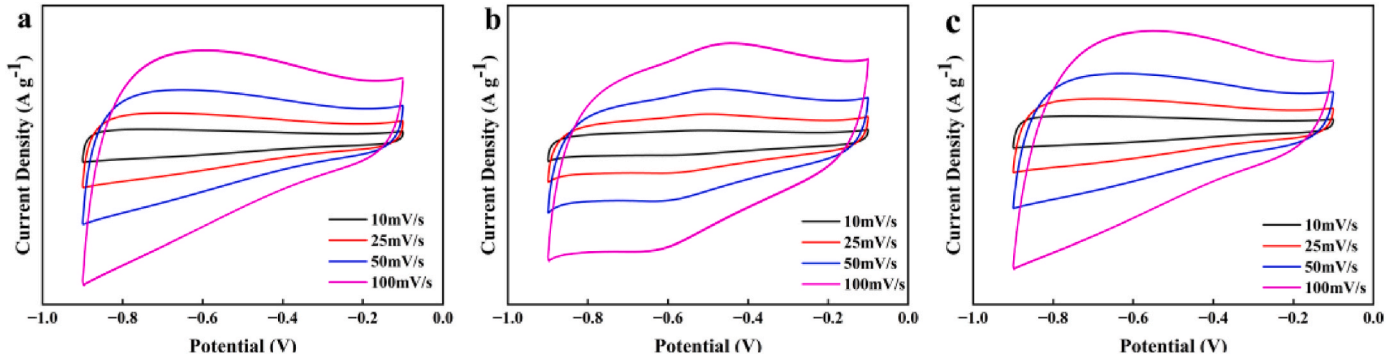

Fig. 8. CV curve of modified biochar (a) PCBC, (b) NPCBC-45, (c) HPCBC-20.

NPCBC-45 was as high as 338.88 F g^{-1} at 1 A g^{-1} current density, an increase of 137.39 %. The pore size structure of NPCBC-45 has not changed significantly, and the oxygen-containing functional groups on the surface provide a large amount of pseudo capacitance for the sample. After HNO_3 activation, although the content of oxygen-containing functional groups of biochar is also greatly increased, the micropore size of sample NPCBC-30 is larger and the number is smaller, and some micropores of sample NPCBC-60 are transformed into mesoporous pores, thus affecting the electrochemical performance of the sample. After H_2O_2 modification, C-O of biochar is oxidized to C=O, the surface

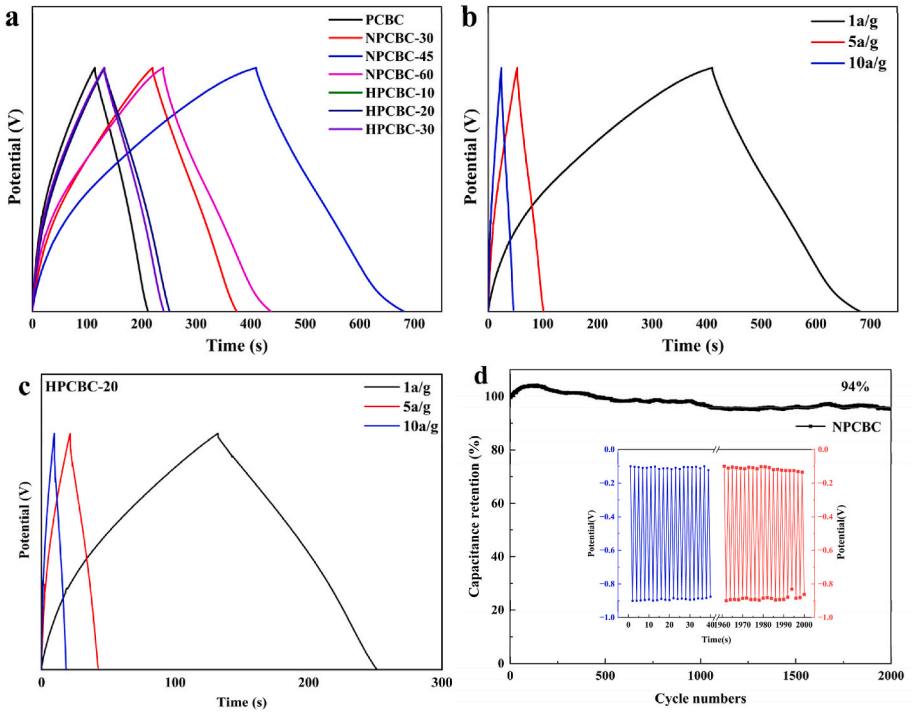

Fig. 9. (a) GCD curve of modified biochar, (b) NPCBC-45, (c) HPCBC-20, (d) Cycle efficiency of supercapacitor.

Table 4
Specific capacitance and internal resistance $F \cdot g^{-1}$.

sample	$C_{1A/g}$	$C_{5A/g}$	$C_{10\ A/g}$	ESR(R Ω)
PCBC	142.75	106.25	91.25	0.46
NPCBC-30	274.88	204.38	185.00	0.70
NPCBC-45	338.88	301.25	278.75	0.87
NPCBC-60	299.63	186.88	152.5	0.74
HPCBC-10	163.88	124.38	107.5	0.56
HPCBC-20	165.00	133.13	117.5	0.55
HPCBC-30	164.13	120.63	103.75	0.58

infiltration of biochar becomes worse, and the equivalent series internal resistance of modified biochar becomes higher, which also leads to better electrochemical performance of biochar under low current density conditions and poor electrochemical performance under high current density conditions. The oxygen-containing functional group content of sample HPCBC-20 did not change, but after the surface modification, the pore structure was improved, and the distribution of micropores was more uniform around 0.91 nm, so the specific capacitance was increased.

3.2.3. *Ac impedance spectrum analysis*

The Nyquist plots of modified biochar electrodes were conducted at the frequency range of 0.01 Hz–100 kHz (Fig. 10(a)). In the low frequency, the Nyquist plots had a semi-circle region which is considered to the contribution of the material's REDOX capacity to the capacitance, indicating good capacitance characteristics of the electrode material. The mid-frequency represents the transformation of the electrode material from capacitance to resistance, and the slope lines of the curve all show a slope of about 45°, responding the diffusion resistance of ions at the electrode/electrolyte interface, known as the "Warburg" impedance [36]. The high-frequency represents resistance and capacitance, and the angle between the straight line and the horizontal axis is called the "phase Angle", and it is generally believed that the closer the "phase Angle" is to 90°, the better the electrochemical performance of the material. As can be seen from Fig. 10(a), the semi-circle diameter of NPCBC-45 is larger than that of HPCBC-20. that is, the REDOX capacity of the biochar modified by HNO_3 contributes the most to the capacitance. All three samples showed a Warburg characteristic 45° slant in the mid-frequency. In the high frequency, the "phase Angle" of the modified biochar was greater than that of the unmodified biochar, that is, the electrochemical performance of the modified biochar had been significantly improved [37].

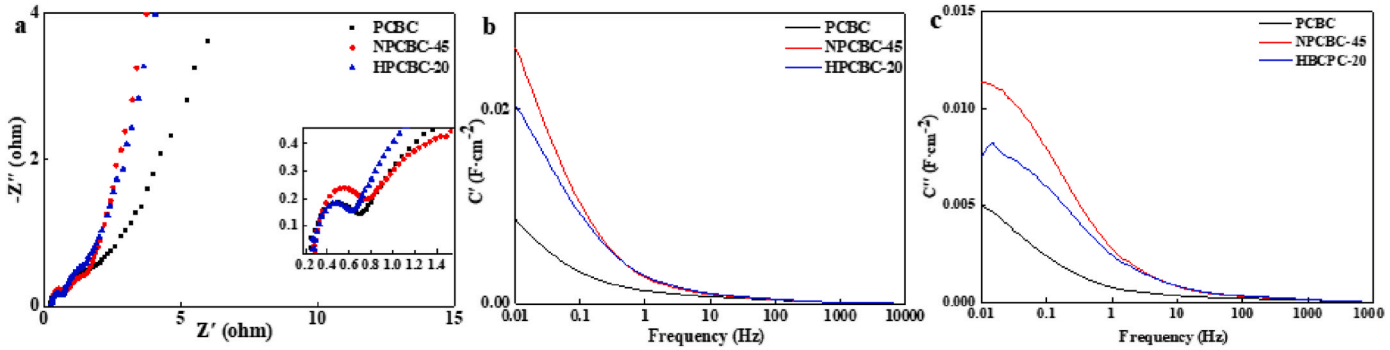

Fig. 10. (a) AC impedance spectrum, (b) Frequency response characteristics, (c) Frequency response characteristics.

Fig. 10(b) and (c) show the frequency response characteristics of the biochar electrode, including real capacitance (C′) and virtual capacitance (C″). Biochar shows pure capacitance behavior in the low frequency region and pure resistance behavior in the high frequency region. From low frequency to high frequency, biochar changes from pure capacitance to pure resistance. Electrolyte ions accumulate in the pores of the electrode material, resulting in capacitance saturation effect, resulting in the capacitance of the real part at low frequency is significantly higher than that at medium frequency and high frequency. Biochar exhibits pure capacitance behavior in the low frequency region and pure resistance behavior in the high frequency region. From low frequency to high frequency, biochar changes from pure capacitance to pure resistance. When the frequency was is greater than 0.1Hz, the real capacitance of biochar decreases significantly, indicating that the material has ideal capacitance behavior. The real capacitance of the modified biochar is higher than that of the unmodified biochar, which is attributed to the further improvement of the pore structure of the modified biochar and the addition of oxygen-containing functional groups to provide additional pseudocapacitance [37].

Due to the complex pore structure of biochar, it is difficult for electrolyte ions to diffuse in the pore structure, and the relaxation time of the double electric layer is long. Therefore, when the frequency is high, the deep pore of biochar is difficult to be utilized, the effective double layer area is low, and the amount of charge stored is limited, resulting in a low specific capacity of biochar in the high frequency region.

4. Conclusion

In conclusion, biochars modified by HNO_3 and H_2O_2 had good electrochemical performance as supercapacitor electrode. HNO_3 modification enhance the content of oxygen-containing functional groups on the surface of biochar and improves the pore structure of biochar through etching. The mesoporosity of biochar was increased by H_2O_2 modification, and the surface oxygen-containing functional groups of modified biochar were mainly C=O. The micropores of NPCBC-45 and HPCBC-20 are concentrated at 0.92 nm and 0.90 nm and the mesoporosity are 33 % and 65 %, respectively. In the three-electrode system, the specific capacitances of NPCBC-45 and HPCBC-20 in 3M KOH electrolyte at $1A{\cdot}g^{-1}$ were 338.88 F g^{-1} and 165.00 F g^{-1}, respectively, which were 2.37 and 1.16 times the capacitance of PCBC, respectively. When the current density increased to 10 A g^{-1}, the specific capacitances were 278.75 F g^{-1} and 117.5 F g^{-1}, respectively, highlighting their excellent electrochemical reversibility and rate characteristics. High surface area, reasonable porous structure and high content of surface oxygen-containing functional groups of modified biochar were responsible for high charge storage capacity. NPCBC-45 has a long cycle stability, and the capacitance retention rate remains at 94 % after 2000 cycles. Therefore, this study has made valuable explorations on the resource utilization of sawdust waste and the development of supercapacitor industry.

CRediT authorship contribution statement

Yang Sun: Writing – review & editing. **Qianqian Yu:** Writing – original draft, Data curation. **Tianhua Yang:** Writing – review & editing, Project administration. **Rundong Li:** Supervision. **Shiyu Zhao:** Data curation.

Data availability

Data will be made available on request.

Declaration of competing interest

The authors declare that they have no known competing financial interests or personal relational relationships that could have appeared to influence the work reported in this paper.

Acknowledgments

The authors gratefully acknowledge the support of the National Natural Science Foundation of China No.52176195) and Liaoning Provincial "Revitalizing Liaoning Talents Plan" Project-Leading Talents in the Hundred Thousand Talents Project XLYC200512.

Appendix A. Supplementary data

Supplementary data to this article can be found online at https://doi.org/10.1016/j.biombioe.2024.107496.

Data availability

No data was used for the research described in the article.

References

[1] T.S. Andrade, J. Vakros, D. Mantzavinos, P. Lianos, Biochar obtained by carbonization of spent coffee grounds and its application in the construction of an energy storage device, Chemical Engineering Journal Advances 4 (2020) 100061, https://doi.org/10.1016/j.ceja.2020.100061.
[2] Y. Li, L. Zhu, J. Shi, Y. Dou, S. Li, R. You, S. Zhang, X. Miao, S. Shi, H. Ji, G. Yang, Super-hydrophilic microporous biochar from biowaste for supercapacitor application, Appl. Surf. Sci. 561 (2021) 150076, https://doi.org/10.1016/j.apsusc.2021.150076.
[3] D.P. Chatterjee, A.K. Nandi, A review on the recent advances in hybrid supercapacitors, J. Mater. Chem. A 9 (29) (2021) 15880–15918, https://doi.org/10.1039/d1ta02505h.
[4] F. Wang, X. Wu, X. Yuan, Z. Liu, Y. Zhang, L. Fu, Y. Zhu, Q. Zhou, Y. Wu, W. Huang, Latest advances in supercapacitors: from new electrode materials to novel device designs, Chem. Soc. Rev. 46 (22) (2017) 6816–6854, https://doi.org/10.1039/c7cs00205j.
[5] A. González, E. Goikolea, J.A. Barrena, R. Mysyk, Review on supercapacitors: technologies and materials, Renew. Sustain. Energy Rev. 58 (2016) 1189–1206, https://doi.org/10.1016/j.rser.2015.12.249.
[6] R. Wang, M. Yao, Z. Niu, Smart supercapacitors from materials to devices, InfoMat 2 (1) (2019) 113–125, https://doi.org/10.1002/inf2.12037.
[7] S. Zhu, J. Ni, Y. Li, Carbon nanotube-based electrodes for flexible supercapacitors, Nano Res. 13 (7) (2020) 1825–1841, https://doi.org/10.1007/s12274-020-2729-5.
[8] S. Zhu, Y. Li, H. Zhu, J. Ni, Y. Li, Pencil-drawing skin-mountable micro-supercapacitors, Small 15 (3) (2018) 1804037, https://doi.org/10.1002/smll.201804037.
[9] S. Rawat, R.K. Mishra, T. Bhaskar, Biomass derived functional carbon materials for supercapacitor applications, Chemosphere 286 (2022) 131961, https://doi.org/10.1016/j.chemosphere.2021.131961.
[10] C. Senthil, C.W. Lee, Biomass-derived biochar materials as sustainable energy sources for electrochemical energy storage devices, Renew. Sustain. Energy Rev. 137 (2021) 110464, https://doi.org/10.1016/j.rser.2020.110464.
[11] L. Luo, Y. Lan, Q. Zhang, J. Deng, L. Luo, Q. Zeng, H. Gao, W. Zhao, A review on biomass-derived activated carbon as electrode materials for energy storage supercapacitors, J. Energy Storage 55 (2022) 105839, https://doi.org/10.1016/j.est.2022.105839.
[12] C. Wang, H. Wang, Performance of C/C electric double layer capacitors with coal-based active carbon electrodes, Ionics 22 (5) (2015) 695–699, https://doi.org/10.1007/s11581-015-1583-z.
[13] J.R. Miller, Perspective on electrochemical capacitor energy storage, Appl. Surf. Sci. 460 (2018) 3–7, https://doi.org/10.1016/j.apsusc.2017.10.018.
[14] I. Michio, K. Hidetaka, O. Tanaike, Carbon materials for electrochemical capacitors, J. Power Sources 195 (24) (2010) 7880–7903, https://doi.org/10.1016/j.jpowsour.2010.06.036.
[15] S.E.M. Pourhosseini, O. Norouzi, H.R. Naderi, Study of micromacro ordered porous carbon with olive-shaped structure derived from Cladophora glomerata macroalgae as efficient working electrodes of supercapacitors, Biomass Bioenergy 107 (2017) 287–298, https://doi.org/10.1016/j.biombioe.2017.10.025.
[16] C. Liu, Q. Li, K. Wang, State-of-charge estimation and remaining useful life prediction of supercapacitors, Renew. Sustain. Energy Rev. 150 (2021) 111408, https://doi.org/10.1016/j.rser.2021.111408.
[17] J. Libich, J. Máca, J. Vondrák, O. Ech, M. Sedlaíková, Supercapacitors: properties and applications, J. Energy Storage 17 (JUN) (2018) 224–227, https://doi.org/10.1016/j.est.2018.03.012.
[18] K.K. Lee, W. Hao, M. Gustafsson, C.W. Tai, D. Morin, E. Björkman, M. Lilliestråle, F. Björefors, A.M. Andersson, N. Hedin, Tailored activated carbons for supercapacitors derived from hydrothermally carbonized sugars by chemical activation, RSC Adv. 6 (112) (2016) 110629–110641, https://doi.org/10.1039/c6ra24398c.

[19] N.K.N. Quach, W.D. Yang, Z.J. Chung, H.L. Tran, The influence of the activation temperature on the structural properties of the activated carbon xerogels and their electrochemical performance, Adv. Mater. Sci. Eng. 2017 (2017) 1–9, https://doi.org/10.1155/2017/8308612.
[20] B. Xu, Y. Chen, G. Wei, G. Cao, H. Zhang, Y. Yang, Activated carbon with high capacitance prepared by NaOH activation for supercapacitors, Mater. Chem. Phys. 124 (1) (2010) 504–509, https://doi.org/10.1016/j.matchemphys.2010.07.002.
[21] L. Wei Qi, Z.M. Chen, X.F. Wang, X.M. Yang, Z.C. Wang, A two-step method for the preparation of high performance corncob-based activated carbons as supercapacitor electrodes using ammonium chloride as a pore forming additive, N. Carbon Mater. 33 (2018) 402–408, https://doi.org/10.1016/j.carbon.2018.11.089.
[22] S. Kumar, G. Saeed, L. Zhu, K.N. Hui, N.H. Kim, J.H. Lee, 0D to 3D carbon-based networks combined with pseudocapacitive electrode material for high energy density supercapacitor: a review, Chem. Eng. J. 403 (2021) 126352, https://doi.org/10.1016/j.cej.2020.126352.
[23] S. Ahmed, M.Y. Bhat, M. Rafat, S.A. Hashmi, Low-temperature thermal exfoliation of graphene oxide for high performance supercapacitor, Materials Science and Surface Engineering (2017) 571–576, 10.jmsse/2348-8956/5-3.5.
[24] Z. Wang, Y. Tan, Y. Yang, X. Zhao, Y. Liu, L. Niu, B. Tichnell, L. Kong, L. Kang, Z. Liu, F. Ran, Pomelo peels-derived porous activated carbon microsheets dual-doped with nitrogen and phosphorus for high performance electrochemical capacitors, J. Power Sources 378 (2018) 499–510, https://doi.org/10.1016/j.jpowsour.2017.12.076.
[25] S. Zhang, C. Wu, W. Wu, C. Zhou, Z. Xi, Y. Deng, X. Wang, P. Quan, X. Li, Y. Luo, High performance flexible supercapacitors based on porous wood carbon slices derived from Chinese fir wood scraps, J. Power Sources 424 (2019) 1–7, https://doi.org/10.1016/j.jpowsour.2019.03.100.
[26] S. Rawat, T. Boobalan, M. Sathish, S. Hotha, B. Thallada, Utilization of CO_2 activated litchi seed biocharforthefabricationofsupercapacitor electrodes. https://dx.doi.org/10.1016/j.biombioe.2023.106747, 2023.
[27] S. Rawat, T. Boobalan, M. Sathish, S. Hotha, B. Thallada, Utilization of CO2 activated litchi seed biochar for the fabrication of supercapacitor electrodes, Biomass Bioenergy 171 (2023) 106747, https://doi.org/10.1016/j.biombioe.2023.106747.
[28] N.F. Sylla, N.M. Ndiaye, B.D. Ngom, B.K. Mutuma, N. Manyala, Ex-situ nitrogen-doped porous carbons as electrode materials for high performance supercapacitor, J. Colloid Interface Sci. 569 (2020) 332–345, https://doi.org/10.1016/j.jcis.2020.02.061.
[29] Y.H. Chiu, L.Y. Lin, Effect of activating agents for producing activated carbon using a facile one-step synthesis with waste coffee grounds for symmetric supercapacitors, J. Taiwan Inst. Chem. Eng. 101 (2019) 177–185, https://doi.org/10.1016/j.jtice.2019.04.050.
[30] Y. Chen, M. Wang, M. Tian, Y. Zhu, X. Wei, T. Jiang, S. Gao, An innovative electro-fenton degradation system self-powered by triboelectric nanogenerator using biomass-derived carbon materials as cathode catalyst, Nano Energy 42 (2017) 314–321, https://doi.org/10.1016/j.nanoen.2017.10.060.
[31] M.Y. Song, Y.H. Zhou, X. Ren, J.F. Wan, Y.Y. Du, Biowaste-based porous carbon for supercapacitor: the influence of preparation processes on structure and performance, J. Colloid Interface Sci. 535 (2018) 276–286, https://doi.org/10.1016/j.jcis.2018.09.055.
[32] Z. Shang, X.Y. An, H. Zhang, M.X. Shen, F. Baker, Y.X. Liu, L.Q. Liu, J. Yang, H. B. Cao, Q.L. Xu, H.B. Liu, Y.H. Ni, Houttuynia-derived nitrogen-doped hierarchically porous carbon for high-performance supercapacitor, Carbon 161 (2020) 62–70, https://doi.org/10.1016/j.carbon.2020.01.020.
[33] N. Shi, Q. Liu, X. He, G. Wang, N. Chen, J. Peng, L. Ma, Molecular structure and formation mechanism of hydrochar from hydrothermal carbonization of carbohydrates, Energy Fuel. 33 (10) (2019) 9904–9915, https://doi.org/10.1021/acs.energyfuels.9b02174.
[34] Q.P. Zhi, Y.S. Wang, X. Bi, T. Zhou, J. Zhou, J.P. Zhao, Z.C. Miao, W.M. Yi, P. Fu, S. P. Zhao, Biochar-based carbons with hierarchical micro-meso-macro porosity for high rate and long cycle life supercapacitors - ScienceDirect, J. Power Sources 376 (2018) 82–90, https://doi.org/10.1016/j.jpowsour.2017.11.077.
[35] M.L. Li, H.Y. Xiao, T. Zhang, Q.R. Li, Y.F. Zhang, Activated carbon fiber derived from sisal with large specific surface area for high-performance supercapacitors, ACS Sustain. Chem. Eng. 7 (5) (2019) 4716–4723, https://doi.org/10.1021/acssuschemeng.8b04607.
[36] Y.L. Huo, Y.J. Gu, Z.L. Chen, X.Y. Ma, F.Z. Wu, X.Y. Dai, Enhanced electrochemical performance of Li1.2Ni0.2Mn0.6-xAlxO2 cathodes in an in situ Li2CO3 coating by a one-step method, Ionics 29 (1) (2023) 71–85, https://doi.org/10.1007/s11581-022-04804-z.
[37] B. Xing, G. Huang, L. Chen, H. Guo, C. Zhang, W. Xie, Z. Chen, Microwave synthesis of hierarchically porous activated carbon from lignite for high performance supercapacitors, J. Porous Mater. 23 (1) (2016) 67–73, https://doi.org/10.1007/s10934-015-0056-0.